Corrosion of Mullite by Molten Salts

Nathan S. Jacobson[*] and Kang N. Lee[*,*]

NASA Lewis Research Center, Cleveland, Ohio   44135

Tetsuo Yoshio[*]

Okayama University, Okayama, Japan

The interaction of molten salts of different Na_2O activities and mullite is examined with furnace and burner tests. The more-acidic molten salts form small amounts of Al_2O_3; the more-basic molten salts form various Na_2O–Al_2O_3–SiO_2 compounds. The results are interpreted using the Na_2O–Al_2O_3–SiO_2 ternary phase diagram, and some possible diffusion paths are discussed. The generally higher melting points of Na_2O–Al_2O_3–SiO_2 compounds lead to better behavior of mullite in molten salts, as compared to SiO_2-protected ceramics such as SiC. Mullite-coated SiC is discussed, and the corrosion behavior is evaluated.

I. Introduction

THE corrosive action of molten salts is a well-known problem for components in combustion environments.[1] Metallic alloys, as well as silicon-based ceramics, are susceptible to this type of corrosion. In the latter case, the process occurs by dissolution of the protective silica (SiO_2) scale to form a nonprotective liquid silicate:[2]

$$2SiO_2(s) + Na_2O(s) \rightarrow Na_2O{\cdot}2SiO_2\ (l) \qquad (1)$$
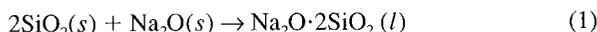
The introduction of alumina to the protective oxide scale leads to higher-melting Na_2O–Al_2O_3–SiO_2 compounds[3] and may provide significantly better corrosion resistance.

This consideration has led us[4,5] and other investigators[6,7] to consider mullite as a protective coating on silicon carbide (SiC). This coating system is attractive, because mullite has a coefficient of thermal expansion that is remarkably similar to that of SiC.[8] The purpose of this paper is to examine the interaction of mullite and mullite-coated SiC with Na_2O at various chemical activities.

This system is best understood with the aid of the Na_2O–Al_2O_3–SiO_2 phase diagram. An isothermal section at 1000°C[3,9] is shown in Fig. 1. The major phases are silica, sodium silicates, mullite, corundum, nepheline ($Na_2O{\cdot}Al_2O_3{\cdot}2SiO_2$), and albite ($Na_2O{\cdot}Al_2O_3{\cdot}6SiO_2$). There also is a high-temperature form of nepheline—carnegieite. However, this should not form at the lower temperatures considered here. Also, many of these phases exist as solid solutions. Mullite and albite exist over a small solid-solution range, and nepheline exists over a larger range. These are shown as tick marks on the composition joins.

There is much information on the corrosion of refractory aluminosilicate compounds by sodium and potassium salts. These studies focus on such applications as glassmelting furnaces and coal gasifiers. Typically, these studies involve large amounts of Na_2O and K_2O at temperatures of 1000°–1500°C.

Farris and Allen[10] have examined the corrosion of aluminosilicate refractories with soda (Na_2O). A major issue was the fluidity of the molten salt and pore penetration, a well-known characteristic of molten salts. In general, the silica component reacts with soda first, and then the alumina component reacts. The major products are nepheline and a compound of composition $3Na_2O{\cdot}2Al_2O_3{\cdot}4SiO_2$. Sodium β-alumina ($11Na_2O{\cdot}Al_2O_3$) formed, but only at temperatures greater than ~1100°C.

Kennedy[11] exposed mullite to soda at 1000°C for 125 h and found carnegieite and sodium β-alumina. He found the volume expansion associated with product formation was the major reason for degradation. Rigby and Hutton[12] have examined corrosion of a series of alumina–silica compositions. For a 60:40 silica:alumina composition at 900° and 1000°C, sodium silicate formed first, followed by the reaction

$$3Al_2O_3{\cdot}2SiO_2 + Na_2O \rightleftharpoons Na_2O{\cdot}Al_2O_3{\cdot}2SiO_2 + 2Al_2O_3$$
$$(2)$$
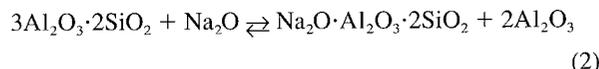
For higher-alumina refractories, $NaAlO_2$ also formed. At temperatures ≥1300°C, sodium β-alumina will form.

Despite the different conditions of these investigations, there are some common observations. Albite has not been observed, although the phase diagram predicts that it is in equilibrium with mullite.[3,9] The phase diagram also indicates that nepheline should not be in equilibrium with mullite, yet these compounds frequently are observed together. Also, sodium β-alumina appears to form only at higher temperatures.

The focus of our research is on ceramics for heat-engine applications. In these cases, the corrodent exists as a thin film of Na_2SO_4 with a low activity of Na_2O. The refractory corrosion literature discussed above is for larger amounts of Na_2O and correspondingly higher chemical activities. Nonetheless, this literature does provide some general guidelines for a heat-engine-directed study.
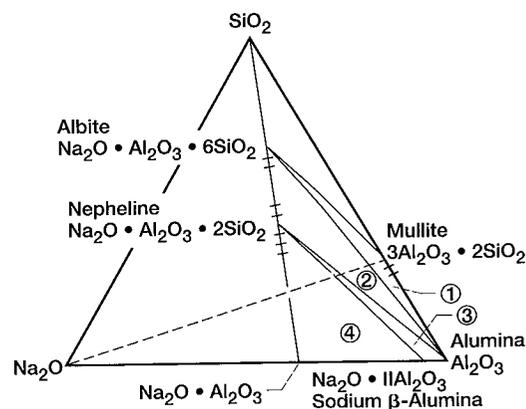
Fig. 1. Isothermal section for $T = 1000$°C of the Na_2O–Al_2O_3–SiO_2 ternary.[3,9] Crosshatched areas indicate solid-solution ranges.
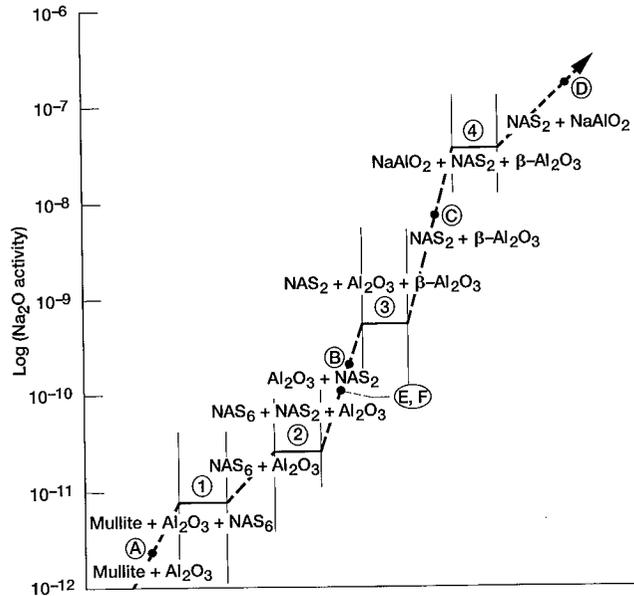
Fig. 2. Activity of Na_2O along dashed line in Fig. 1 at 1000°C. Abbreviations are N, Na_2O; A, Al_2O_3; and S, SiO_2. Circled numbers refer to the compatibility triangles in Fig. 1; circled letters refer to the experimental conditions in Table II.

Here, the reactions of mullite and mullite-coated SiC with controlled activities of Na_2O in both laboratory and jet-fuel burner experiments are examined. The mechanism of these reactions will be discussed in terms of the Na_2O–Al_2O_3–SiO_2 ternary phase diagram.

II. Thermodynamic Considerations

The critical issue in these experiments is the thermodynamic activity of Na_2O, a_{Na_2O}.[2] A high activity of Na_2O is termed a basic molten salt, and a low activity of Na_2O is termed an acidic molten salt. This Na_2O activity can be set by using thin films of Na_2CO_3 and Na_2SO_4 and an overpressure of $CO_2(g)$ or $SO_3(g)$, respectively:

Table I. Composition of Bulk Mullite

Element	Amount (wt%)
Aluminum	30.6
Calcium	0.03
Copper	0.01
Iron	0.3
Sodium	0.06
Oxygen	bal.
Lead	0.8
Silicon	15.9
Titanium	0.07
Yttrium	0.03
Zinc	0.01
Zirconium	0.4

$$Na_2CO_3(l) \leftrightarrows Na_2O(s,l) + CO_2(g)$$
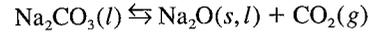
$$(a_{Na_2O} = K_3/p_{CO_2} = 8.06 \times 10^{-7}/p_{CO_2} \text{ at } 1000°C) \quad (3)$$

$$Na_2SO_4(l) \leftrightarrows Na_2O(s,l) + SO_3(g)$$
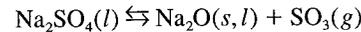
$$(a_{Na_2O} = K_4/p_{SO_3} = 4.06 \times 10^{-16}/p_{SO_3} \text{ at } 1000°C) \quad (4)$$

K_3 and K_4 are the equilibrium constants for reactions (3) and (4), respectively, and have been calculated from the thermochemical tables.[13] The chemical activity of Na_2CO_3 and Na_2SO_4 are taken as unity, because these are essentially pure phases. However, Na_2CO_3 still decomposes to a greater extent than Na_2SO_4 and forms a more basic salt.

The dashed line in Fig. 1 represents the addition of Na_2O to mullite. Movement toward pure Na_2O represents increasing the activity of Na_2O through a series of compatibility triangles, labeled as 1, 2, 3, and 4 in Fig. 1. The Na_2O activity in each triangle was determined from the following equilibria:

$$Na_2O + 3(3Al_2O_3 \cdot 2SiO_2) \rightleftarrows$$

$$Na_2O \cdot Al_2O_3 \cdot 6SiO_2 + 8Al_2O_3$$
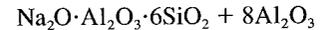
(Triangle 1: mullite/albite/alumina)

$$2(Na_2O \cdot Al_2O_3 \cdot 6SiO_2) + 4Na_2O + 4Al_2O_3 \rightleftarrows$$

$$6(Na_2O \cdot Al_2O_3 \cdot 2SiO_2)$$
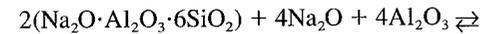
(Triangle 2: albite/nepheline/alumina)

Table II. Summary of Experimental Conditions, Phases Predicted from an Ideal Diffusion Path, and Phases Observed

Condition*	Description of experimental condition	Calculated partial pressure (bar) p_{SO_2}	p_{SO_3}	Calculated activity of Na_2O, a_{Na_2O}	Predicted phases	Observed phases
A	Furnace; Na_2SO_4/930 ppmv SO_2–O_2 atmosphere, 1000°C, 24 h	8.1×10^{-4}	1.2×10^{-4}	3.6×10^{-12}	Mullite, Al_2O_3, Na_2SO_4	Mullite, Na_2SO_4, Al_2O_3
B	Furnace; Na_2SO_4/11.56 ppmv SO_2–O_2 atmosphere, 1000°C, 24 h	1.0×10^{-5}	1.5×10^{-6}	2.7×10^{-10}	Mullite, Al_2O_3, $Na_2O \cdot Al_2O_3 \cdot 6SiO_2$, $Na_2O \cdot Al_2O_3 \cdot 2SiO_2$, Na_2SO_4	Mullite, Na_2SO_4, Al_2O_3, $Na_2O \cdot Al_2O_3 \cdot 2SiO_2$
C	Furnace; Na_2SO_4/11.56 ppmv SO_2–O_2 atmosphere, 1089°C, 24 h	1.1×10^{-5}	8.7×10^{-7}	1.8×10^{-8}	Mullite, Al_2O_3, $Na_2O \cdot Al_2O_3 \cdot 6SiO_2$, $Na_2O \cdot Al_2O_3 \cdot 2SiO_2$, Na β-Al_2O_3, Na_2SO_4	Mullite, Na_2SO_4, Al_2O_3, $3Na_2O \cdot 2Al_2O_3 \cdot 4SiO_2$
D	Furnace; Na_2CO_3/1 bar CO_2 atmosphere, 1000°C, 24 h			8.1×10^{-7}	Mullite, Al_2O_3, $Na_2O \cdot Al_2O_3 \cdot 6SiO_2$, $Na_2O \cdot Al_2O_3 \cdot 2SiO_2$, Na β-Al_2O_3, $Na_2O \cdot Al_2O_3$	Mullite, $Na_2O \cdot Al_2O_3 \cdot SiO_2$
E	Burner; 2 ppmw sodium, 0.05% sulfur in fuel, fuel:air = 0.025, 1000°C, 4 bar, 40 h	2.7×10^{-5}	4.0×10^{-6}	1.0×10^{-10}	Mullite, Al_2O_3, $Na_2O \cdot Al_2O_3 \cdot 6SiO_2$, $Na_2O \cdot Al_2O_3 \cdot 2SiO_2$, Na_2SO_4	Mullite, Na_2SO_4
F	Burner; 2 ppmw sodium, 0.05% sulfur in fuel, fuel:air = 0.025, 1000°C, 4 bar, 40 h	2.7×10^{-5}	4.0×10^{-6}	1.0×10^{-10}	Mullite, Al_2O_3, $Na_2O \cdot Al_2O_3 \cdot 6SiO_2$, $Na_2O \cdot Al_2O_3 \cdot 2SiO_2$, Na_2SO_4	Mullite, Na_2SO_4

*Conditions A–E are for bulk mullite; condition F is for SiC and mullite-coated SiC.
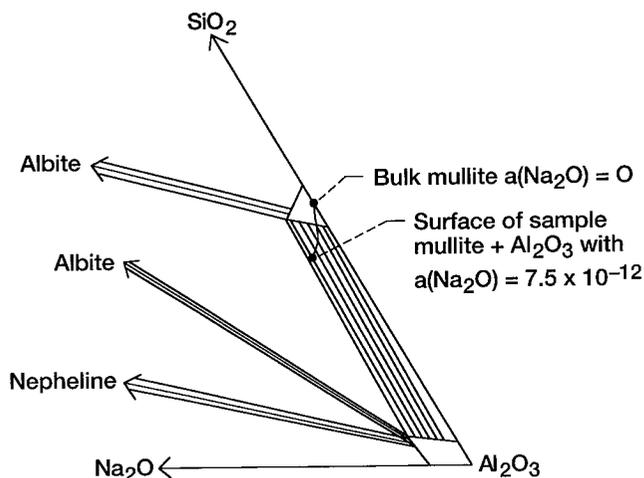
Fig. 3. Probable diffusion path for the reaction of mullite and Na_2O, with $a_{Na_2O} = 3.6 \times 10^{-11}$ (condition A in Table II).

$$Na_2O + 11Al_2O_3 \rightleftarrows Na_2O \cdot 11Al_2O_3$$
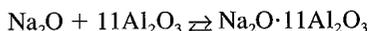
(Triangle 3: nepheline/alumina/sodium β-alumina)

$$10Na_2O + Na_2O \cdot 11Al_2O_3 \rightleftarrows 11(Na_2O \cdot Al_2O_3)$$

(Triangle 4: nepheline/sodium β-alumina/
$Na_2O \cdot Al_2O_3$)

Only two phases are necessary to set the Na_2O activity for triangles 3 and 4. Thermodynamic data[13,14] can be used to set up a plot of activity of Na_2O versus composition from the above equilibria, as shown in Fig. 2 for 1000°C. This analysis assumes stoichiometric compounds with no solid solubility, which is not the case for many of these, particularly $Na_2O \cdot Al_2O_3 \cdot 2SiO_2$. These calculations do predict that for low Na_2O activities, sodium aluminosilicates will form, and, for the higher Na_2O activities, the compounds sodium β-alumina and sodium aluminate will form. This is consistent with the refractory corrosion literature that involves high Na_2O activities and often produces sodium aluminates.

The heat-engine studies discussed here involve low activities of Na_2O. In our studies, the Na_2O is not depleted, and we can regard this system as a diffusion couple of Na_2O and mullite. There are many detailed studies of analogous metallurgical systems.[15] The three oxides—Na_2O, Al_2O_3, and SiO_2—are the three components of this system. If temperature, pressure, and composition are fixed, the phase rule then indicates that two-phase regions are possible in the product layer between the Na_2O and mullite. From the composition of these regions, delineation of some diffusion paths should be possible. Complications arise from the unknown identity of the diffusing species and extensive solid-solution formation in this system.

III. Experimental Procedure

The bulk mullite specimens were sintered from a powder made by a coprecipitation method (Tosoh Soda Co., Tokyo, Japan). A typical atomic emission analysis is shown in Table I. Coupons were cut to ~2.0 cm × 0.4 cm × 0.3 cm and ground with 15 μm diamond. One piece was polished further to a 1 μm finish with diamond paste and examined with the scanning electron microscope (SEM). There was no evidence of a second phase.

In addition, some mullite-coated SiC was examined. Sintered α-SiC with carbon and boron additives (Carborundum Co., Niagara Falls, NY) was used as the substrate of the same approximate dimension given above and coated on all six faces. The plasma-spray process used to deposit the mullite coating has been described in previous publications.[4,5] It was shown that a thermal-shock-resistant coating can be applied by heating the substrate to ensure that the mullite retains its crystallinity.

Both the bulk and coated specimens were exposed to corrosive atmospheres in a laboratory furnace and a jet-fuel burner. These techniques have been described elsewhere.[2] Briefly, heated coupons were air-brushed with an aqueous solution of Na_2SO_4 or Na_2CO_3. After the solution dried on the coupons, a film of salt remained. Dry salt loadings of 2–3 mg/cm² were used for all coupons. Two to four coupons were examined for each condition. The coupons then were placed in a laboratory furnace with a fixed gas atmosphere at 1000° or 1089°C, which set the activity of Na_2O as shown in reactions (3) and (4) above. A free-energy minimization computer code[16] was used to calculate the values of equilibrium p_{SO_2}, p_{SO_3}, and a_{Na_2O} for our furnace exposures; the inputs were the salt and gas atmosphere. The experimental conditions are summarized in Table II.
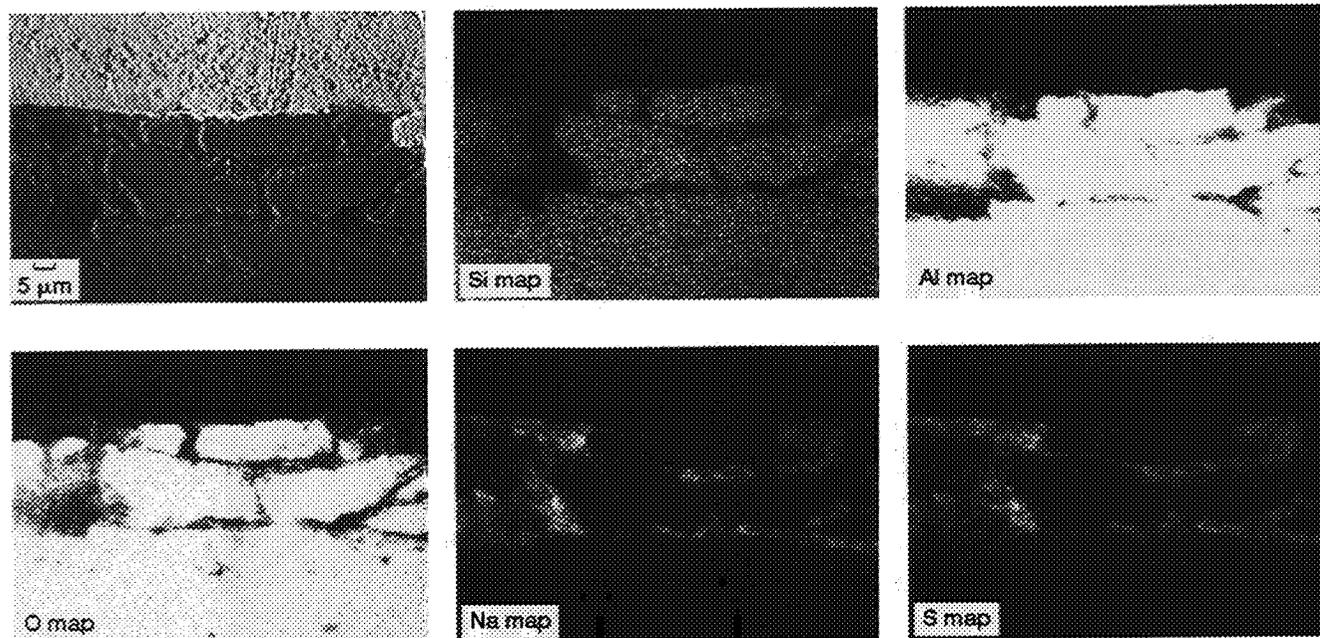
Fig. 4. Polished cross section and associated elemental dot maps for the reaction of mullite and Na_2O, with $a_{Na_2O} = 2.9 \times 10^{-10}$ (condition B in Table II).

XRD: Mullite, Al_2O_3, NAS_2, Na_2SO_4
EDS: Na, O, Si, Al, S

5 μm

↓ 1 hr boiling water

XRD: Mullite
EDS: O, Si, Al

5 μm
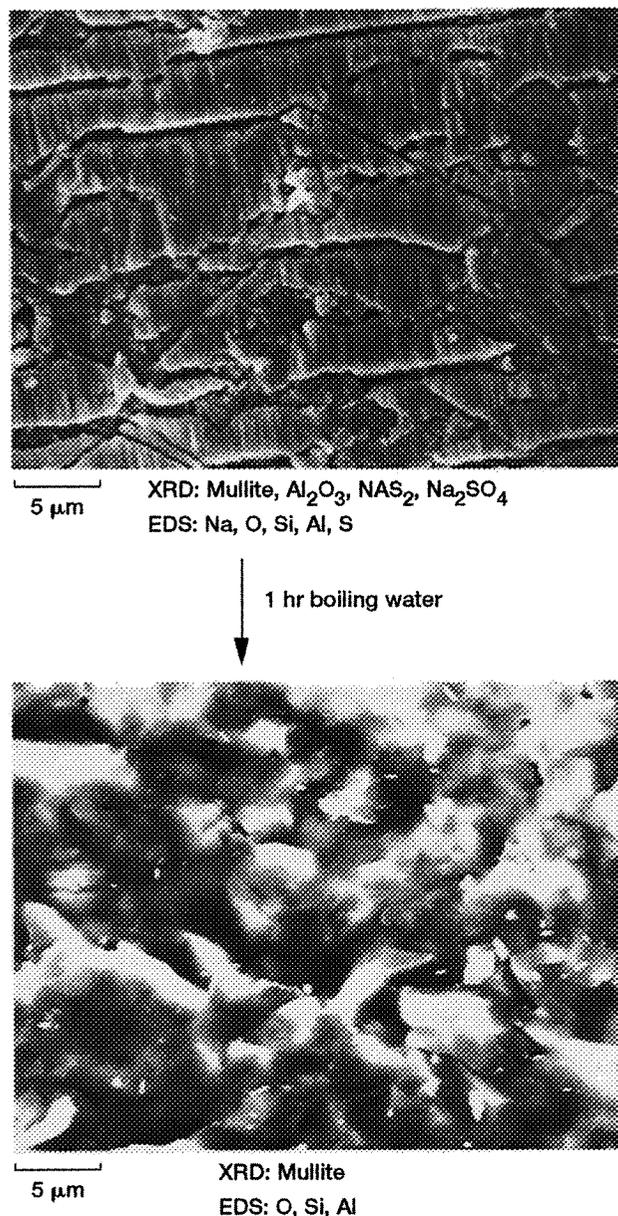
Fig. 5. Sequential removal of product layers for the reaction of mullite and Na_2O, with $a_{Na_2O} = 2.9 \times 10^{-10}$ (condition B in Table II).

The burner conditions also have been described previously.[17] These consist of a 4 atm (~0.4 MPa) pressurized burner using Jet A fuel. Salt was added as NaCl, which reacts with sulfur impurities in the fuel to form a Na_2SO_4 deposit.[18] This type of situation simulates the actual corrosion process that occurs in a heat engine. Using the NASA Chemical Equilibrium Code,[19] estimation of the p_{SO_3} generated in such a burner (2 ppm sodium, 0.05% sulfur, Jet A fuel) and then calculation of the activity of Na_2O was possible. This information is given in Table II.

After exposure to these environments, the specimens were cooled and analyzed via several techniques. X-ray diffraction (XRD) was used to identify the crystalline phases. Even though there are many $Na_2O–SiO_2–Al_2O_3$ compounds in the XRD card files, there was not always a clear match of our XRD scans to those on file. In addition, glasses may form from some of these compounds and would not be identifiable by XRD. Elemental analysis was helpful in these cases. Polished cross sections were prepared by sputter-coating samples with gold and then electroplating with a few millimeters of nickel or copper. Then, the sample was polished with diamond paste using ethylene glycol as a lubricant to preserve the water-soluble phases. The
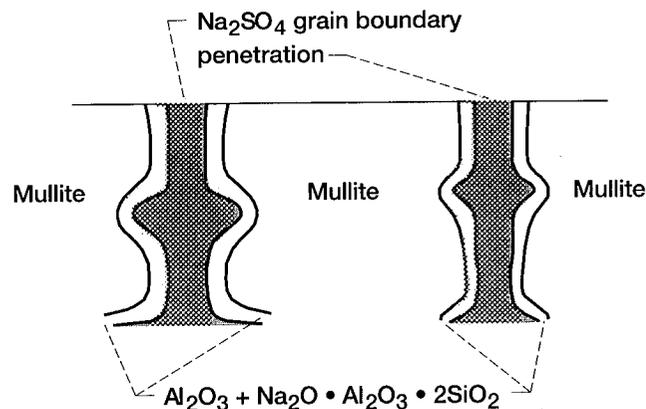
Fig. 6. Inferred cross-sectional structure of sample shown in Fig. 4.

thick conductive coating allowed electron optic examination and analysis through the entire thickness of the corrosion product. The sections were examined with an SEM equipped for energy-dispersive spectroscopy (EDS) and electron probe microanalysis (EPMA). For the EPMA measurements, the aluminum standard was Al_2O_3, the silicon standard was SiO_2, the sodium standard was NaF, and the oxygen standard was MgO.

IV. Results and Discussion

(1) Furnace Studies

Table II lists the predicted phases and observed products. Each of these experiments will be discussed, beginning with the most-acidic salt.

Condition A is the most-acidic salt, with $a_{Na_2O} = 3.6 \times 10^{-12}$. XRD results indicated the presence of mullite, Na_2SO_4, and a small amount of Al_2O_3. A surface examination of the specimen in conjunction with EDS indicated an outer layer of condensed liquid Na_2SO_4, which is an effective source of Na_2O. The Na_2SO_4 was removed by dissolution in boiling water, revealing a rough surface with some degree of etching. XRD of this surface indicated only mullite. Apparently, the water-soluble layer contained Na_2SO_4 and Al_2O_3 (very likely as small particles).

From Fig. 2, the first three-phase region—mullite/alumina/albite—occurs when $a_{Na_2O} = 7.5 \times 10^{-12}$. The experimental conditions are less than this, so that only mullite and alumina are expected, as shown in Table II. These two phases have been observed experimentally. A proposed diffusion path is shown in Fig. 3, with the two-phase region between mullite and alumina enlarged to some solubility of Na_2O.
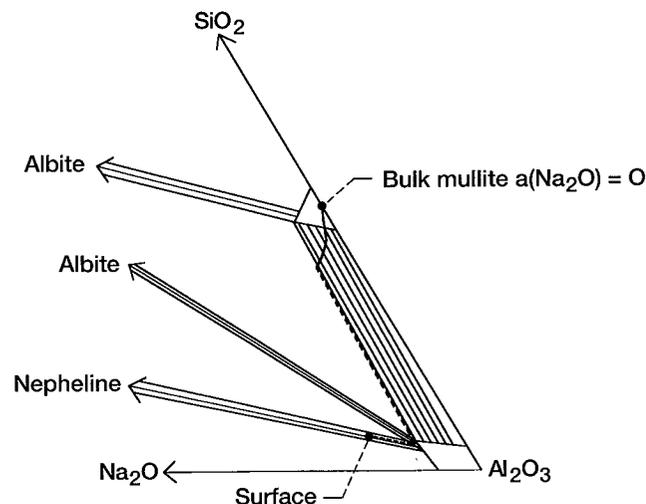
Fig. 7. Probable diffusion path for reaction examined in Fig. 4.
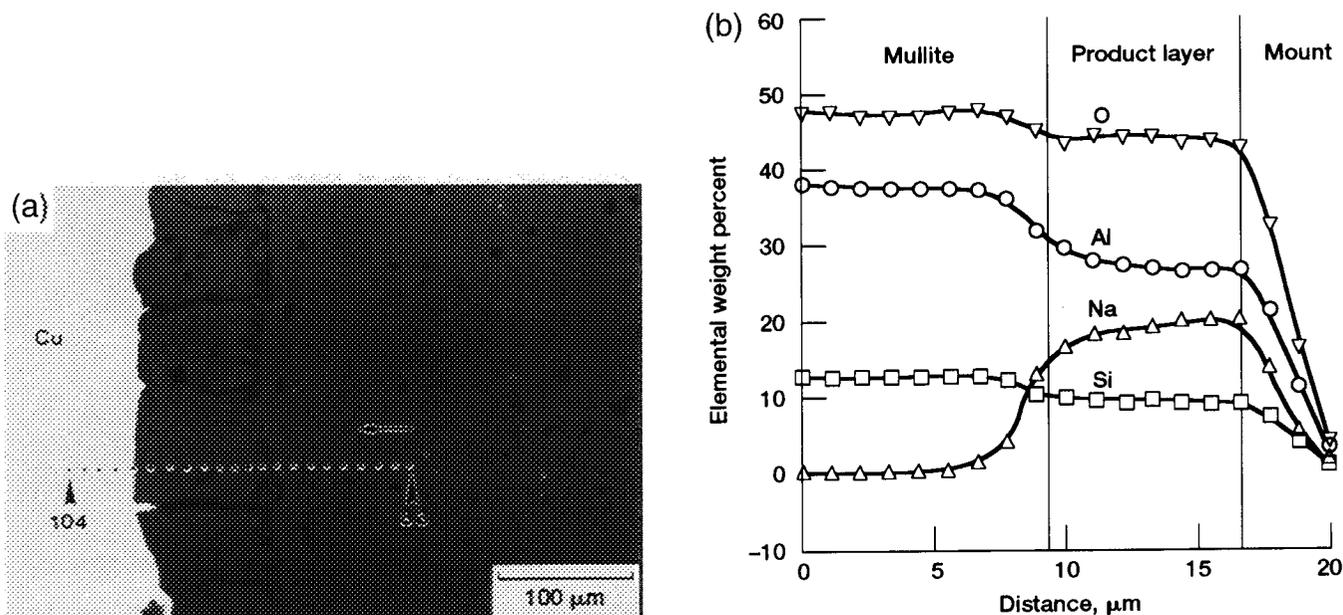
Fig. 8. EPMA of mullite reacted with Na_2CO_3 in 1.0 bar (10^5 Pa) CO_2 for 24 h at 1000°C (condition D in Table II) ((a) polished cross section and (b) quantitative elemental concentration profile).

Decreasing the amount of SO_2 to 11.56 ppm at 1000°C decreased the amount of SO_3 and then, according to Eq. (4), increased a_{Na_2O}. This is condition B in Table II, with a_{Na_2O} = 2.9×10^{-10}. In this case, XRD showed mullite, Al_2O_3, Na_2SO_4, and a very small amount of $Na_2O \cdot Al_2O_3 \cdot 2SiO_2$. No $Na_2O \cdot Al_2O_3 \cdot 6SiO_2$ was detected. A polished cross section and associated X-ray dot maps are shown in Fig. 4. The corrosion-affected zone did not form a continuous product layer but rather a number of discontinuous regions 10–25 μm thick, with the corrosion-affected zone separated from the bulk by the predominately Na_2SO_4 melt. Na_2SO_4 may initially attack the grain boundaries of the mullite, and then the melt may surround the grains or collections of grains. The grain size of the mullite was several micrometers, which is consistent with intergranular attack in Fig. 4.

To reveal more information about these corrosion products, the surfaces were examined in the SEM before and after a boiling-water treatment. This is shown in Fig. 5. Before the boiling-water treatment, the surface primarily was solidified Na_2SO_4, as indicated by EDS analysis and XRD. After treatment in boiling water, the diffraction peaks for Na_2SO_4, Al_2O_3, and $Na_2O \cdot Al_2O_3 \cdot 2SiO_2$ disappeared, leaving only mullite peaks. Apparently, the melt that surrounded the mullite grains in Fig. 4 contained Na_2SO_4, Al_2O_3, and $Na_2O \cdot Al_2O_3 \cdot 2SiO_2$, which again was an effective source of Na_2O. The limits of resolution of our microprobe did not allow us to distinguish these products.

A proposed cross-sectional structure from the outer melt layer to the mullite is shown schematically in Fig. 6. Figure 7 shows a probable diffusion path; this is idealized, because the
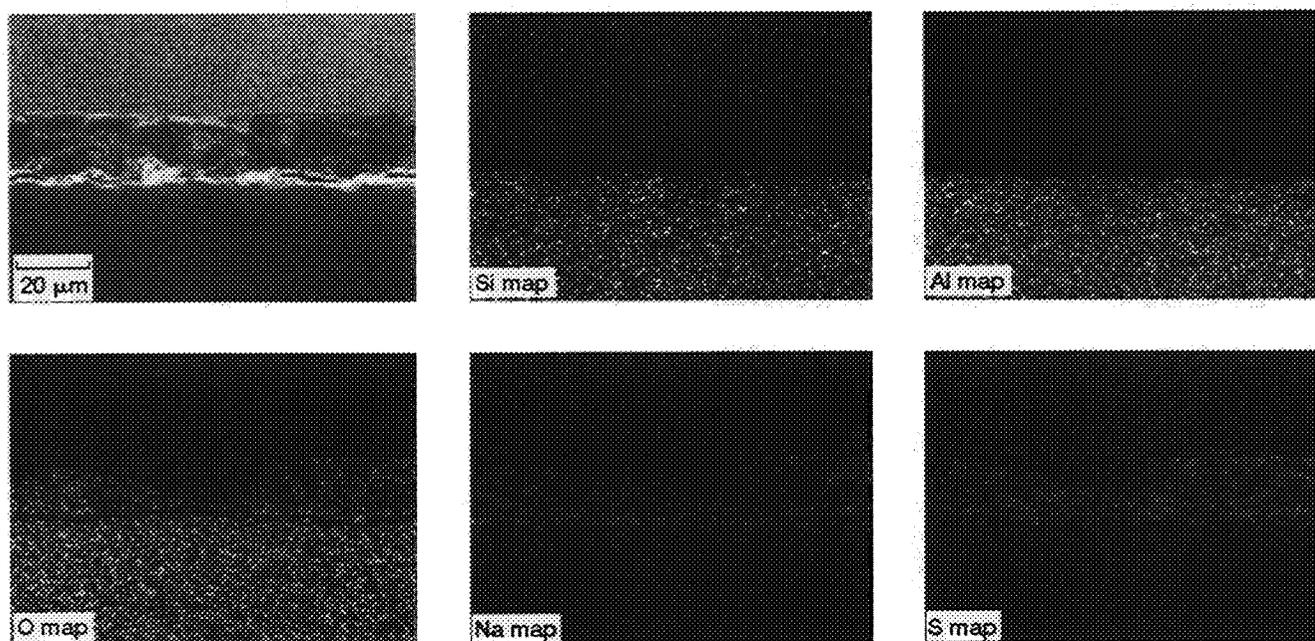
Fig. 9. Polished cross section and associated elemental maps for mullite reacted in the burner with a fuel-to-air ratio of 0.025, Jet A fuel (0.05% sulfur), 2 ppm sodium as NaCl for 40 h at 1000°C, and 4 atm (~0.4 MPa) (condition E in Table II).
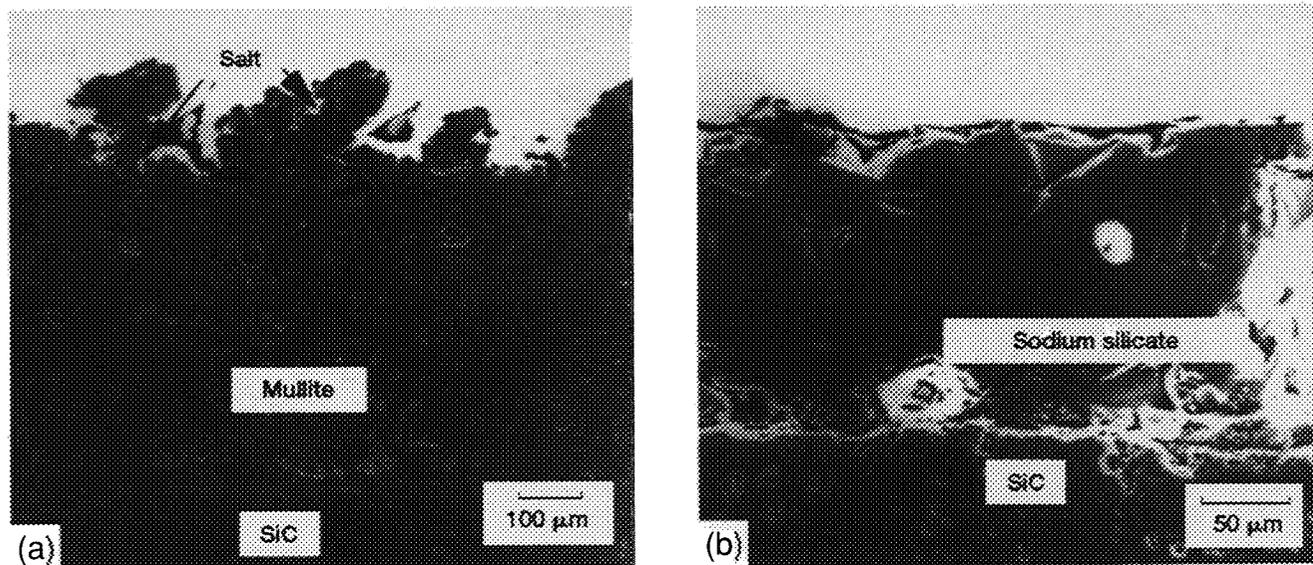
Fig. 10. Polished cross section after burner exposure; fuel-to-air ratio of 0.025, Jet A fuel, 2 ppm sodium as NaCl, 40 h at 1000°C, and 4 bar (condition F in Table II) ((a) uncoated SiC and (b) SiC with mullite coating).

routes are shown along joins. Inititially, some of the SiO_2 from the mullite is attacked by Na_2O, leaving Al_2O_3. The initial removal of SiO_2 is consistent with the refractory corrosion studies of Rigby and Hutton,[12] and Fig. 3 shows it as the diffusion path from the mullite to the pure Al_2O_3. By moving down to this region, the diffusion path can bypass the mullite/alumina/albite and alumina/albite/nepheline compatibility triangles and move directly to the alumina/nepheline two-phase region. Some kinetic barrier to forming albite seems to exist, which is consistent with the refractory corrosion literature, as discussed in the Introduction. The primary product between the mullite and Na_2O then is a two-phase mixture of Al_2O_3 and $Na_2O \cdot Al_2O_3 \cdot 2SiO_2$.

For condition C in Table II, the activity of Na_2O was altered by increasing the temperature to 1089°C and keeping the amount of SO_2 at 11.56 ppm, which leads to an a_{Na_2O} value of 1.3×10^{-8}. XRD now showed Na_2SO_4, mullite, oriented Al_2O_3, and $3Na_2O \cdot 2Al_2O_3 \cdot 4SiO_2$, which is analogous to the situation described above, but with a slightly different sodium aluminosilicate composition.

Condition D in Table II is a more-basic molten salt—Na_2CO_3 in 1 atm CO_2. After only ~5 min, the Na_2CO_3 layer was

not detectable anymore. This indicated that Na_2O completely reacted with the mullite, and instead of a diffusion-couple situation, a condensed phase reaction of Na_2O and mullite existed. After 24 h of reaction, a product layer ~15 μm thick formed. A polished cross section and associated quantitative microprobe trace is shown in Fig. 8. The estimated error in the elemental analysis was ±1.5%, primarily because of the porosity of the mullite. Converting the data to moles of the individual components form indicated that the product layer was $1.2Na_2O \cdot 1.5Al_2O_3 \cdot 1SiO_2$. XRD showed the best match with the compound $Na_2O \cdot Al_2O_3 \cdot SiO_2$, in reasonable agreement with the EPMA data.

The layer of sodium aluminosilicate has uniform composition. When this layer reaches the mullite, there is a concentration decrease in the ratio of sodium to mullite. There may be some penetration of the mullite by sodium, which is expected because mullite can transport sodium cations.[18,20]

(2) Burner Studies

An actual corrosion situation is a hot flame seeded with salt that reacts with sulfur fuel impurities, leading to Na_2SO_4 deposits on the components. As discussed, this is best simulated
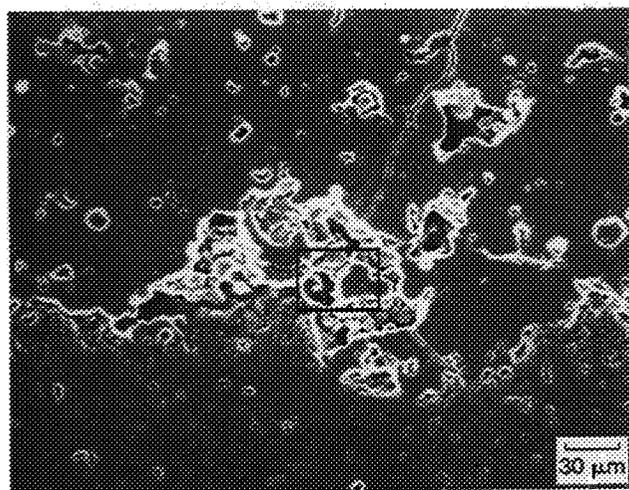
(a)
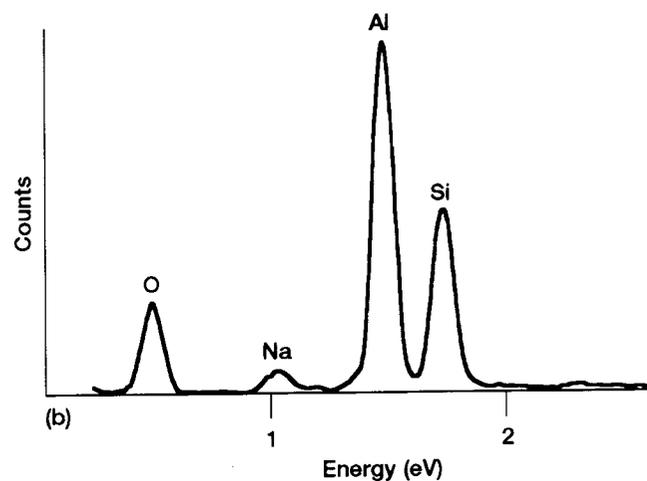
(b)

Fig. 11. SiC with mullite coating. Mullite/SiC interface fuel-to-air ratio of 0.025, Jet A fuel, 2 ppm sodium as NaCl, 40 h at 1000°C, and 4 bar (condition F in Table II) ((a) polished cross section and (b) EDS trace, showing presence of sodium).

with a burner. Despite the complexity of a burner, determination of some basic chemical parameters and performance of an analysis similar to that conducted for the furnace are possible. As indicated in Table II, this produced an acidic salt deposit with $a_{Na_2O} = 1.0 \times 10^{-10}$. Results were similar to the furnace tests with acidic salts.

A polished cross section is shown in Fig. 9, which clearly shows a layer of Na_2SO_4 on mullite, as indicated by the sulfur elemental dot map. There was no evidence of reaction, and, unlike the furnace situation, Al_2O_3 was not detected in XRD. Al_2O_3 may have formed only in very small quantities.

A polished cross section of mullite-coated SiC after burner treatment, test condition F in Table II, is shown in Fig. 10(a); this is compared to a coupon of uncoated SiC after a similar treatment, shown in Fig. 10(b). The mullite-coated SiC clearly shows substantially better behavior. The uncoated SiC forms a thick sodium silicate layer, whereas the mullite-coated material shows essentially no reaction. An examination of the mullite surface shows no evidence of reaction; only a small amount of Na_2SO_4 has deposited in the asperities.

There seems to be no reaction in this case. However, Na_2O eventually will diffuse through the mullite and reach the mullite/SiC interface. Figure 11 shows the mullite/SiC interface and an associated EDS trace, which indicates the presence of sodium. As mentioned, mullite is well-known to be a good conductor for sodium.[18,20] There are two driving forces for sodium diffusion through mullite: the activity gradient in sodium and sodium silicate formation. After long-term exposure, a liquid sodium silicate very likely will form at the mullite/SiC interface, which may lead to coating spallation. For long-term operation in sodium-containing atmospheres, a mullite coating is only a partial solution. Additional coating layers, which are better barriers to sodium, are necessary.[21]

V. Summary and Conclusions

The interaction of Na_2O with mullite and mullite-coated SiC has been examined. Mullite generally behaves better in Na_2O-containing environments than pure SiO_2 because of the formation of higher-melting Na_2O–Al_2O_3–SiO_2 compounds. The actual products are explained in terms of the thermodynamics of the system and diffusion paths in the Na_2O–Al_2O_3–SiO_2 ternary. The more-aggressive burner tests are generally consistent with the furnace tests. The improved corrosion resistance of mullite and close coefficient of thermal expansion match to that of SiC make it a suitable protective-coating material. Over short terms, it looks quite promising. However, for longer times or in a high-sodium

environment, the transport of sodium through mullite is a likely problem.

References

[1]F. S. Pettit and C. S. Giggins, "Hot Corrosion"; pp. 327–54 in *Superalloys II.* Edited by C. T. Sims, N. S. Stoloff, and W. C. Hagel. Wiley, New York, 1987.

[2]N. S. Jacobson, J. L. Smialek, and D. S. Fox, "High-Temperature Corrosion of Engineering Ceramics"; pp. 514–47 in *Corrosion of Glass, Ceramics, and Ceramic Superconductors.* Edited by D. E. Clark and B. K. Zoitos. Noyes, Park Ridge, NJ, 1992.

[3]E. M. Levin, C. R. Robbins, and H. F. McMurdie, *Phase Diagrams for Ceramists*; p. 181. American Ceramic Society, Columbus, OH, 1964.

[4]K. N. Lee, R. A. Miller, and N. S. Jacobson, "A New Generation of Plasma-Sprayed Mullite Coatings on Silicon Carbide," *J. Am. Ceram. Soc.*, **78** [3] 705–10 (1995).

[5]K. N. Lee, R. A. Miller, and N. S. Jacobson, "Plasma-Sprayed Mullite Coatings on Silicon-Based Ceramics," U.S. Pat. No. 08/031,444, 1995.

[6]J. I. Federer, "Alumina Base Coatings for Protection of SiC Ceramics," *J. Mater. Eng.*, **12** [2] 141–49 (1990).

[7]J. R. Price, M. Van Roode, and C. Stala, "Ceramic Oxide-Coated Silicon Carbide for High-Temperature Corrosive Environments," *Key Eng. Mater.*, **72–74**, 71–84 (1992).

[8]Y. S. Touloukian, R. K. Kirby, R. E. Taylor, and T. Y. R. Lee, *Thermal Expansion of Nonmetallic Solids.* Plenum, New York, 1977.

[9]J. J. Brown Jr., "The Use of Phase Diagrams to Predict Alkali Oxide Corrosion of Ceramics"; pp. 43–84 in *Phase Diagrams in Advanced Ceramics.* Edited by A. Alper. Academic Press, New York, 1994.

[10]R. E. Farris and J. E. Allen, "Aluminous Refractories—Alkali Reactions," *Iron Steel Eng.*, **50** [2] 67–74 (1973).

[11]C. R. Kennedy, "Alkali Attack on a Mullite Refractory in the Grand Forks Energy Technology Center Slagging Gasifier," *J. Mater. Energy Syst.*, **3**, 27–31 (1981).

[12]G. R. Rigby and R. Hutton, "Action of Alkali and Alkali-Vanadium Oxide Slags on Alumina–Silica Refractories," *J. Am. Ceram. Soc.*, **45** [2] 68–73 (1962).

[13]I. Barin, *Thermochemical Properties of Inorganic Substances, Parts I and II.* VCH Verlagegesellschaft, Wieheim, Germany, 1989.

[14]F. A. Elrefaire and W. W. Smeltzer, "The Stability of β-Al_2O_3 ($Na_2O \cdot 11Al_2O_3$) in Oxygen Atmospheres," *J. Electrochem. Soc.*, **128** [7] 1443–47 (1981).

[15]F. J. J. van Loo, "Multiphase Diffusion in Binary and Ternary Solid-State Systems," *Prog. Solid State Chem.*, **20**, 47–99 (1990).

[16]HSC Chemical Reaction and Equilibrium Software, Outokumpu Research, Pori, Finland, 1990.

[17]N. S. Jacobson, C. A. Stearns, and J. L. Smialek, "Burner Corrosion of SiC at 1000°C," *Adv. Ceram. Mater.*, **1** [2] 154–61 (1986).

[18]N. S. Jacobson, "Sodium Sulfate: Deposition and Dissolution of Silica," *Oxid. Met.*, **31** [1/2] 91–103 (1989).

[19]S. Gordon and B. J. McBride, "Computer Program for Calculation of Complex Chemical Equilibrium Compositions, Rocket Performance, Incident and Reflected Shocks, and Chapman-Jouguet Detonations," NASA Rept. No. SP-273, 1971.

[20]G. W. Watt, R. E. Andresen, and R. A. Rapp, "A Comparison of Reference Electrodes in Molten Sodium Sulfate"; p. 81 in *Molten Salts.* Edited by J. Braunstein and J. R. Selman. Electrochemical Society, Princeton, NJ, 1981.

[21]K. N. Lee, N. S. Jacobson, and R. A. Miller, "Refractory Oxide Coatings on SiC Ceramics," *MRS Bull.*, **19** [10] 35–38 (1994).   □